Frontiers in Heat and Mass Transfer (FHMT), 18, 16 (2022)
DOI: 10.5098/hmt.18.16

Global Digital Central
ISSN: 2151-8629

Frontiers in Heat and Mass Transfer

Available at www.ThermalFluidsCentral.org

CORRELATION DEVELOPMENT FOR JET IMPINGEMENT HEAT TRANSFER AND FORCE ON A MOVING CURVED SURFACE

Ali Chitsazan[a], Georg Klepp[a], Birgit Glasmacher[b]

[a]*Institute for Energy Research, Ostwestfalen-Lippe University of Applied Sciences and Arts, Lemgo 32657, Germany*
[b]*Institute for Multiphase Processes, Leibniz University Hannover, Hannover 30167, Germany*

ABSTRACT

The effect of jet Reynolds number, jet exit angle, the nozzle to surface distance, jet to jet spacing on the heat transfer, and pressure force performance from multiple impinging round jets on a moving curved surface have been numerically evaluated. Two correlations are developed and validated for the average Nu number and the pressure force coefficient and the agreement between the CFD and correlations was reasonable. The surface motion effect becomes more pronounced on the Nu number distribution for low jet Re number, high jet to jet spacing, large jet to surface distance, and angled jets. The pressure force coefficient is highly dependent on the jet to surface distance and jet angle but relatively insensitive to jet Re number and jet to jet spacing.

Keywords: Angled jets, Heat transfer, Pressure force, Surface motion, Curvature, Correlation

1. INTRODUCTION

Jet impingements enhance the heat transfer rate in many industrial applications such as cooling, heating, and drying due to the large amounts of heat and mass transfer between the surface and the working fluid. Jet impingement flow has many applications in the industry such as the cooling of electronic and turbine components, drying of textile and paper, etc.

Ito et al. (2007) observed that the Nusselt number for both flat and concave surfaces increased as the Re number increased. Li and Corder (2008) found that the secondary peak on the curved surface is seen for the small jet to plate distance (H/d), and the case with a small distance shows a higher heat transfer rate downstream. Ashok Kumar et al. (2009) observed that the average heat transfer coefficient on the curved surface reduces as H/d increases beyond unity. Heo et al. (2012) observed that the heat transfer rate increases with the pitch of orthogonal jet nozzles on a target curved surface. Bu et al. (2015) found that decreasing the surface curvature and increasing the jet impingement angle can improve the Nu number at the stagnation point. Fenot et al. (2008) found that increasing the curvature causes a small growth of Nu number in the impingement region and the curvature produces confinement of the jet flow that decreases the Nu number distribution.

Some industrial processes such as paper dryer or rolling of sheet stock or external heat transfer to rotating parts require the target surface to move. The selection of an effective speed depends on several factors such as the jet spacing and a time constant associated with the heat and mass transfer rate to or from the target surface. Chattopadhyay (2006) found that the surface velocity affects strongly the flow field over the target surface and reduces the heat transfer rate. Kadiyala and Chattopadhyay (2017) observed that by increasing the surface velocities the heat transfer reduces initially and reaches a minimum and increases again. Maximum heat transfer is achieved for the stationary surface before the transition, while the maximum heat transfer after the transition is achieved at the velocity ratio equal to 6.

Jet impingement force is very important in drying applications for force-sensitive products (i.e. paper, fabrics) or force-sensitive surfaces (i.e. painted, coated). Wang et al. (2015) found that the mean impact force coefficients from a single circular jet impinging normally onto a fixed flat surface are highly dependent on the nozzle to surface distance, but relatively insensitive to the jet Reynolds number. Kastner et al. (1988) calculated the jet impingement force through the integration of the measured pressure distributions on flat plates due to an impinging jet. Page et al. (1989) deduced experimentally that wall pressure distribution, reattachment angle, and reattachment radius of radial jet flow are independent of the jet Reynolds number. A dimensionless force coefficient has been defined by Page et al. (1990) to describe the net surface force of radial jet flows. The radial jet nozzles with flow exit angles of -10° in paper machines increase the sheet stability owing to the suction forces (Thiele et al., 1993; Thiele et al., 1995). Peper et al. (1997) found that the total force exerted by radial jets on a plane surface is lower than that exerted by inline jets and the total force exerted by radial jets decreases with decreasing the flow exit angle.

Chitsazan et al. (2020) conducted a numerical investigation of jet impingement heat transfer and force on a moving flat surface for different jet Re numbers, nozzle to surface distance, jet to jet spacing, jet exit angle, and surface velocity.

The above works focus on the round jets impinging on either the fixed curved surface or moving flat surface and there is not observed any investigation concerning the effect of multiple jets impinging on a moving curved surface. The heat transfer between multiple jets and a moving curved surface is more difficult to study due to the changing boundaries and effect of surface curvature but is also very relevant in engineering applications such as the drying process. The scope of this research is to investigate numerically the effect of jet Reynolds number, nozzle to surface distance, jet to jet spacing, and jet exit angle on the heat transfer and pressure force from multiple impinging round jets on a moving curved surface. Two correlations are developed and validated for the average Nusselt number and the force coefficient as a function of jet Re number, nozzle to surface distance (H/d), jet to jet spacing (S/d), jet exit angle (θ), relative surface velocity (VR) and relative curvature (Cr). This work contributes to a better understanding of the jet impingement heat transfer and pressure force on a moving curved surface, which can lead to the optimal design of the industrial drying application.

Global Digital Central
ISSN: 2151-8629

2. EQUATIONS AND SOLUTION METHODS

2.1 Mathematical Formulation

In the following, the conservation laws of mass, momentum, and energy are expressed for an incompressible fluid with the constant fluid properties in steady state form:

$$\frac{\partial U_i}{\partial X_i} = 0 \tag{1}$$

$$U_j \frac{\partial U_i}{\partial X_j} = \frac{\partial}{\partial X_j}\left(\nu \frac{\partial U_i}{\partial X_j} \right) - \frac{1}{\rho}\frac{\partial P}{\partial X_j} \tag{2}$$

$$U_j \frac{\partial \Theta}{\partial X_j} = \frac{\partial}{\partial X_j}\left(\Gamma_\Theta \frac{\partial \Theta}{\partial X_j} \right) + q_\Theta \tag{3}$$

The Reynolds-Averaged Navier Stokes equations are solved for the transport of mean flow quantities with appropriate RANS turbulence models to describe the influence of the turbulent quantities to provide closure relations. Each solution variable in the instantaneous Navier-Stokes equations should be decomposed into an averaged value and a fluctuating component to obtain the Reynolds-Averaged Navier-Stokes equations. The resulting equations for the mean quantities are essentially identical to the original equations, except that an additional term now appears in the momentum transport equation. This additional term, known as the Reynolds stress tensor, has the following definition:

$$T_t = -\overline{U_i' U_j'} \tag{4}$$

The challenge is thus to model the Reynolds stress tensor to close the time-averaged equations. Eddy viscosity models employ the concept of a turbulent viscosity for modeling of Reynolds stress tensor. The most common model is known as the Boussinesq approximation:

$$T_t = 2\nu_t S_{ij} - \frac{2}{3}\delta_{ij} k \tag{5}$$

Where ν_t is the turbulent viscosity, k is the turbulence kinetic energy, δ_{ij} is the Kronecker delta (=1 if i=j, otherwise =0) and S_{ij} is mean strain rate tensor and given by:

$$S_{ij} = \frac{1}{2}\left(\frac{\partial \overline{U}_i}{\partial X_j} + \frac{\partial \overline{U}_j}{\partial X_i} \right) \tag{6}$$

Since the assumption that the Reynolds stress tensor is linearly proportional to the mean strain rate and does not consider the anisotropy of turbulence, some two-equation models extend the linear approximation to include the non-linear constitutive relations. The use of hybrid models as a combination of efficient two-equation models is advisable. The Shear Stress Transport (SST) k-ω model as a combination of the k-ε model in the freestream and the standard k-ω model in the inner parts of the boundary layer is an obvious choice. For further details, refer to the STAR-CCM$^+$ user guide.

2.2 Definition of Characteristic Numbers

The local heat transfer coefficient is nondimensionalized to the Nusselt number by the following expression:

$$Nu = \frac{hd}{k_t} = \frac{q}{(T_w - T_j)} \cdot \frac{d}{k_t} \tag{7}$$

Where q is the convective heat flux, T_w is the target wall temperature, T_j is the jet exit temperature, d is the jet exit diameter, k_t is the thermal conductivity of the air at jet exit temperature and h is heat transfer coefficient.

Pressure force on the surface is the force that the fluid exerts in the normal direction to the surface. Jet impingement force is presented in dimensionless form by a force coefficient C_f and defined as follows:

$$C_f = \frac{F}{0.5\rho V^2 (\pi d^2/4)} \tag{8}$$

Where F is the pressure force on the surface, ρ is the density of the fluid, d is the diameter of the nozzle and V is the jet exit velocity. The pressure force on the surface is computed as:

$$F = P_{st} A \tag{9}$$

Where P_{st} is the pressure at the stagnation point and A is the surface area.

2.3 Domain and Boundary Condition

Figure 1 shows the geometry of the multiple impinging jets and boundary conditions used. All jet inlets were modeled as circular planes in the top wall. The incoming jet flow is assumed to be with constant fluid properties at T_j = 298.15 K, entered with a uniform velocity profile. For all configurations, the pattern was regular. The target surface as a moving curved surface was modeled as a no-slip wall held at a constant temperature of Tw = 333.15 K. No-slip with adiabatic wall boundary conditions is imposed on all other solid surfaces. Constant pressure outlet boundary condition is applied to all open boundaries. The movement of the curved surface is considered along curvilinear axes. Symmetric boundary condition was also applied in the X-Y plane for the central jet to reduce the computational cost.

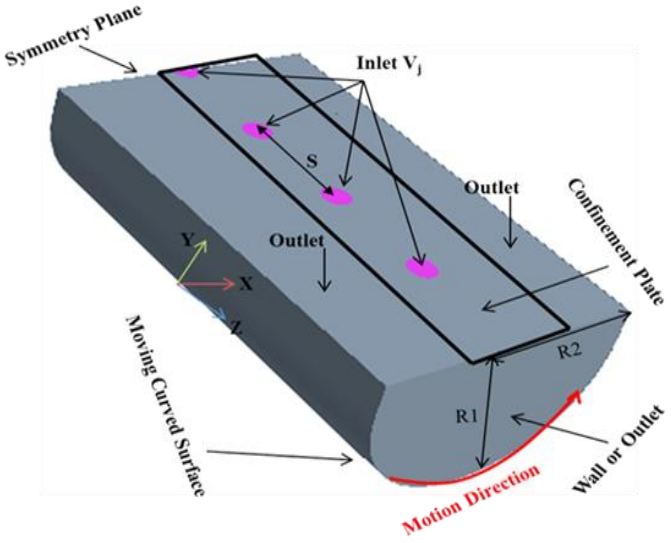

Fig. 1 Schematic of the computational domain

The relative surface curvature (Cr) is defined as the ratio of the minor radius (R_1=40mm) to the major radius (R_2=50mm) and the relative

Global Digital Central
ISSN: 2151-8629

surface velocity is defined as the ratio of surface velocity to jet velocity. Details of the parameters investigated are presented in Table 1.

Table 1 Parameters investigated for a real industrial dryer

Parameters	Values
Number of jet rows	1
Number of jets in each row	3
Jet exit diameter (d)	10 mm
Jet Reynolds number (Re)	1980, 10000, 23000, 40000, 66200
Relative nozzle to surface distances (H/d)	1, 2, 5, 10, 15, 20
Relative jet to jet spacing (S/d)	2, 4, 6, 10
Jet exit angle (θ)	45, 60 , 90 (°)
Relative surface curvature (Cr)	0.8
Relative surface velocity (VR)	0.28
Surface temperature	333.15 K
Inlet Jet temperature	298.15 K

2.4 Computational Detail

The CFD model is set up and run with the commercial code STAR-CCM$^+$ 13.02.013. The final solution was obtained by applying a second-order discretization upwind scheme, and the SIMPLE algorithm is used for pressure-velocity coupling. SST k-ω turbulence model is used as recommended by many researchers (Heo et al., 2012; Kadiyala and Chattopadhyay 2017). The flow in the near-wall regime was simulated using a low-Reynolds number approach. The solution was considered to be converged when the value of the scaled residual of the continuity, momentum, and energy equations is less than 10^{-4}.

2.5 Grid Generation and Sensitivity

An unstructured polyhedral grid was generated using STAR-CCM+. A boundary layer with a dimensionless wall distance of less than one was built on the target surface. The grid was refined near the target surface to enable better resolution of the flow in this part (see Figure 2).

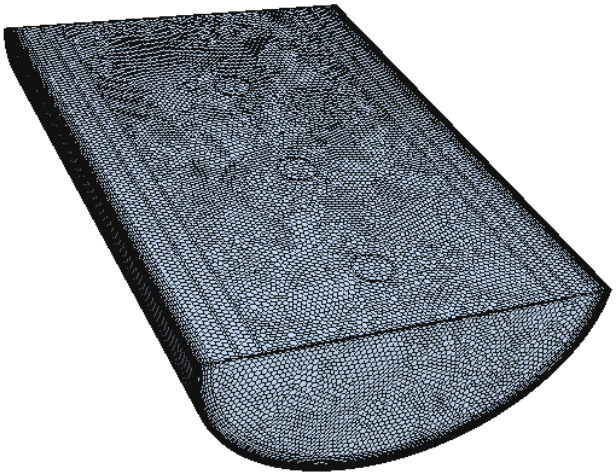

Fig. 2 3 D view of the computational grid

The grid sensitivity study is carried out by analyzing the variation of the local Nu distribution on the target surface along the Z-centerline (the lines pass through the stagnation points of jets). The local discretization error distribution is calculated by applying the GCI method (Roache, 2003). The overall discretization error for the fine and intermediate grid (2.6 and 4.12% respectively) was very small. The intermediate grid is selected as the final grid to reduce the computational cost (see Table 2).

Table 2 Grid parameters of the refinement study

Grid	Base size (m)	Cell number	Max y_1^+	Average GCI %
Course	0.00192	447,431	0.44	---
Intermediate	0.00127	970,045	0.31	4.12
Fine	0.00088	2,157,431	0.23	2.6

3. RESULTS AND DISCUSSION

3.1 Evaluation of Computational Model

Figure 3 indicates the local Nu along the curvilinear axis on the target surface. The numerical results of this work have been compared with the experimental data of Fenot (2008). The agreement between the two is very good and closely followed the same trend.

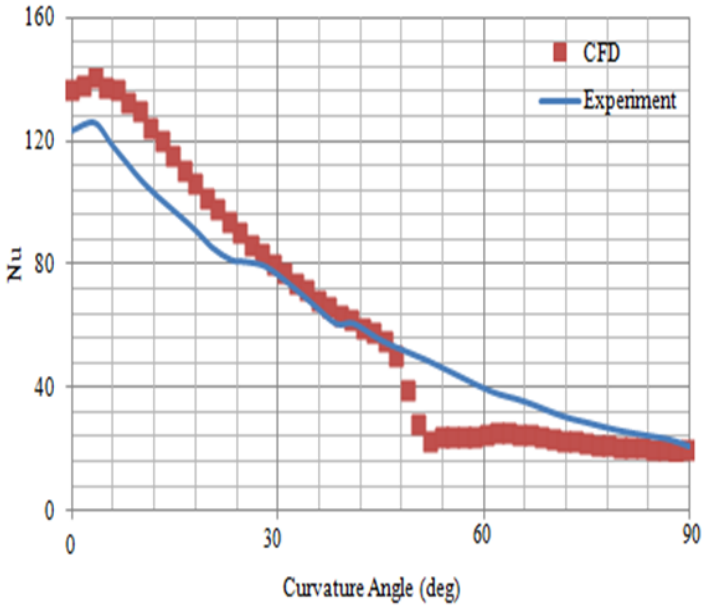

Fig. 3 Comparison of the local Nu along the curvilinear axis on a fixed curved surface between experiments and CFD (H/d=5, S/d=4, Re = 23000, Cr=1, θ=90; and VR=0)

3.2 Jet Reynolds Number (Re)

3.2.1 Effect on Heat Transfer

Figure 4 compares the effect of Reynolds number on the total average Nusselt number on a moving curved surface. The results show that the average Nusselt number increased as the Reynolds number increased from 1980 to 66200. That is because a higher jet Reynolds number corresponds to a higher jet exit velocity and the strong flow acceleration associated with the higher jet velocities contributes greatly to the heat transfer enhancement (see Fig.5). This result is in agreement with the finding of Chitsazan et al. (2020) for jet impingement heat transfer on a flat surface.

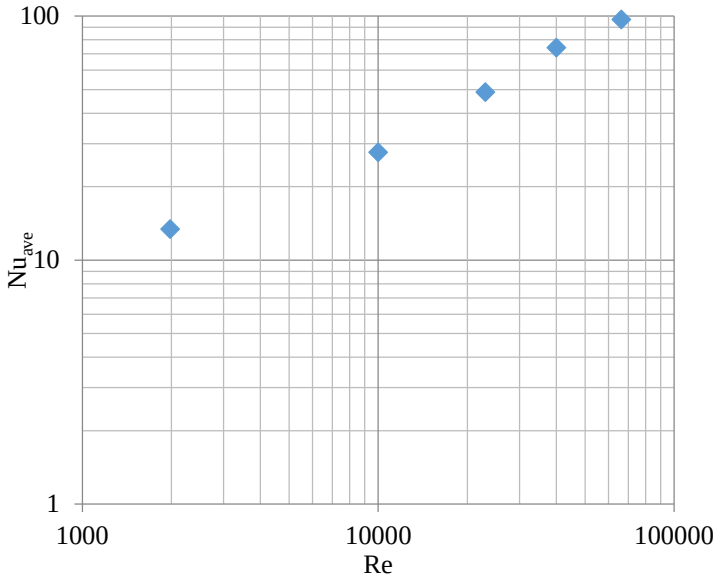

Fig. 4 Effects of jet Re number on the average Nu in logarithmic scale (H/d=2, S/d=4, and VR=0.28)

The surface motion reduces the effectiveness of each jet and the surface motion effects become more pronounced as the jet Reynolds number decreases. Therefore, the surface motion has no significant effect on the Nusselt number distribution on a moving curved surface at a high jet Reynolds number (see Fig. 5). Hence, there is a more uniform heat transfer for jets at low Reynolds number (e.g. Re=1980 and10000) on a moving curved surface. Thus the importance of surface motion to optimize the heat transfer due to an array of impinging jets is reduced at high jet Reynolds number (Re>10000).

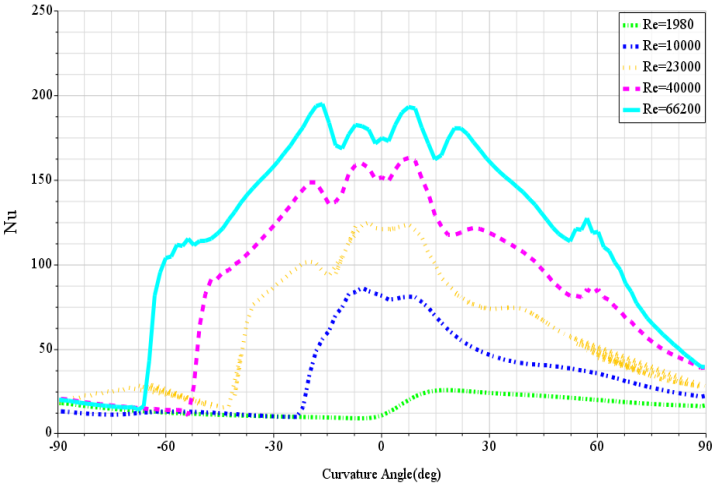

Fig. 5 Effect of jet Re number on the local Nu along curvilinear axes (H/d=2, S/d=4, and VR=0.28)

3.2.2 Effect on Pressure Force

Figure 6 compares the effect of jet Re number on the pressure force coefficient on a moving curved surface. Increasing the jet Re number occurs with increasing the jet exit velocity from the nozzle and also jet force. Due to the definition of the pressure force coefficient (see Eq. 8), the pressure force coefficient is relatively insensitive to the jet Reynolds number. This result is in agreement with the findings of Chitsazan et al. (2020) for jet impingement force on a flat surface.

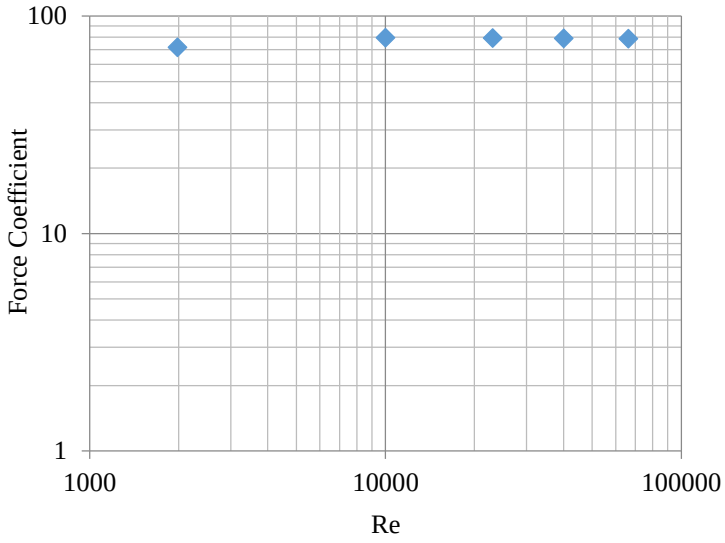

Fig. 6 Effect of jet Re number on the pressure force coefficient (H/d=2, S/d=4, and VR=0.28)

3.3. Nozzle to Surface Distance (H/d)

3.3.1 Effect on Heat Transfer

Figure 7 compares the effect of the nozzle to surface distance (H/d) on the total average Nusselt number on a moving curved surface. The results show that the average Nusselt number varies quite strongly with H/d and the average Nu increases as H/d decreases. Because the adjacent jet interference before impingement causes significant degradation of the heat transfer in the stagnation region (see Fig. 8). However, the adjacent jet interference before impingement is minimized as the H/d is decreased to one and the higher average Nu number is obtained when H/d =1 compared to other cases. This result is in agreement with the finding of Chitsazan et al. (2020) for jet impingement heat transfer on a flat surface.

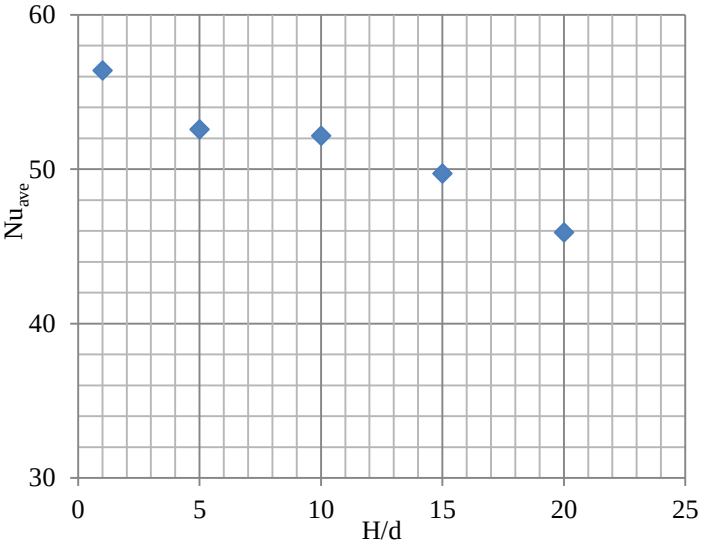

Fig. 7 Effects of the nozzle to surface on the average Nu (Re=23000, S/d=4, and VR=0.28)

As the H/d decreases, the jet interaction on the target surface increases significantly around Z/d =2. Hence, further reducing the value of H/d to 1 creates a significant nonuniform distribution in the local Nusselt number over the target surface (see Fig. 8).

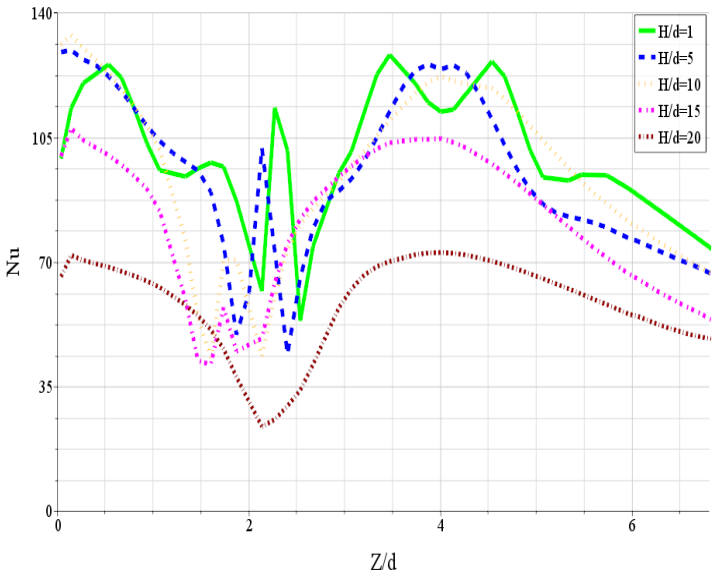

Fig. 8 Effect of the nozzle to surface distance on the local Nu along Z-axis (Re=23000, S/d=4, VR=0.28)

The surface motion has more effect on the Nusselt number distribution on a moving curved surface at high values of H/d and there is a more uniform heat transfer for jets at high values of H/d (15 and 20). Because the flow in the case of low H/d (1 and 5) has more momentum compared to the higher H/d (see Fig. 9). Thus the importance of surface motion to optimize the heat transfer due to an array of impinging jets is reduced when the surface is in low H/d (1-10).

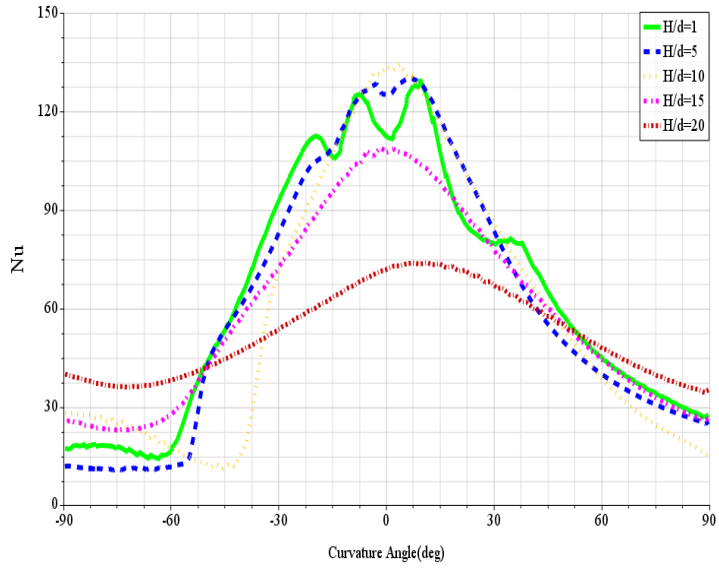

Fig. 9 Effects of the nozzle to surface distance on the local Nu along curvilinear axes (Re=23000, S/d=4, VR=0.28)

3.3.2 Effect on Pressure Force

Figure 10 compares the effect of the nozzle to surface distance (H/d) on the pressure force coefficient on a moving curved surface. Results indicate that the pressure force coefficients on the target surface are highly dependent on the nozzle to surface distance.

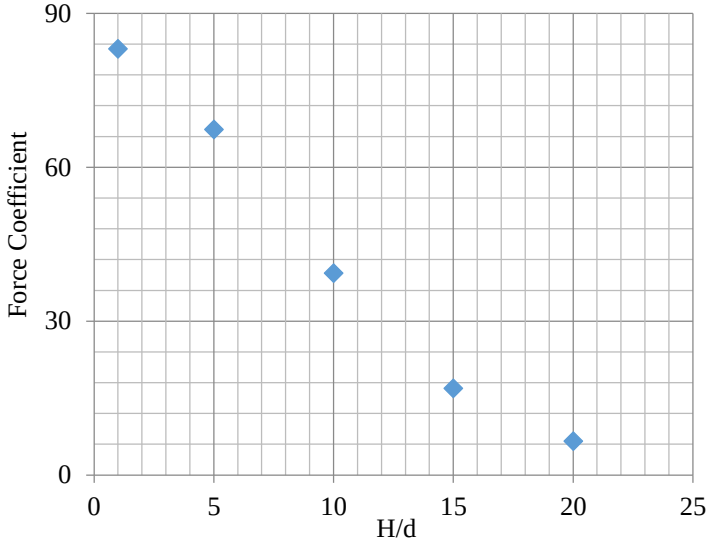

Fig. 10 Effect of the nozzle to surface distance on the pressure force coefficient (Re=23000, S/d=4, and VR=0.28)

The pressure force coefficients increase with decreasing the H/d due to the decrease in the momentum exchange between the jet flow and the ambient leading to the increase in the pressure on the impingement surface (see Fig.11). That's why the identification of optimum H/d is very important for the sensitive product to the pressure force such as paper. This result is in agreement with the findings of Chitsazan et al. (2020) for jet impingement force on a flat surface.

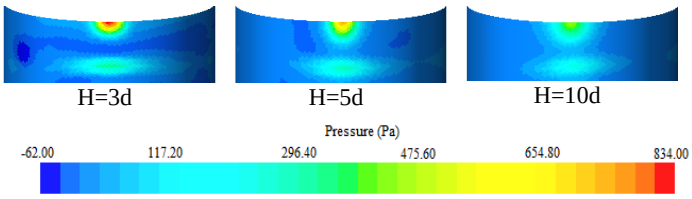

Fig. 11 Pressure distribution from central jet impinging on a moving curved surface for different H/d (Re=23000, S/d=4, VR=0.28, and θ=90°)

3.4 Jet to Jet Spacing (S/d)

3.4.1 Effect on Heat Transfer

Sketch of the different configurations with the inline arrangement and different jet to jet spacing are shown in Figure 12. The diameter of each round orifice (d) through a confinement plate with the constant length 14d is 10 mm. All configurations have the same array of 1 row with different jet to jet distance over the range of S/d=2-10 and jet to surface distance H/d=2. There is no change in the averaging area among the cases.

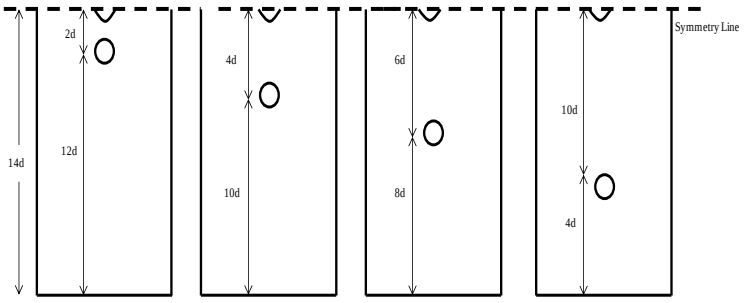

Fig. 12 Sketch of the different jet to jet spacing

Figure 13 compares the effect of the jet to jet spacing (S/d) on the total average Nusselt number on a moving curved surface. The area-averaged Nusselt number sharply decreases with a decrease in the jet to jet spacing. The minimum Nusselt number is found in the lower jet to jet spacing (S/d = 2) compared to the other cases.

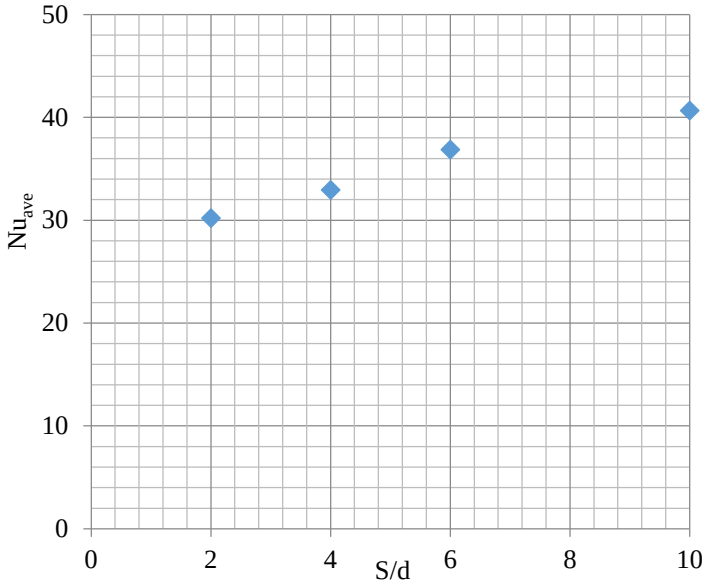

Fig. 13 Effect of the jet to jet spacing on the average Nu (Re=23000, H/d=2, VR=0.28)

As the jet to jet spacing decreases the wall flows of the two jets are impinging upon each other and forming a new stagnation region (Z/d~1, 2.5, 3.2, 5). This affects the stagnation and average heat transfer coefficients (see Fig. 13 and 14).

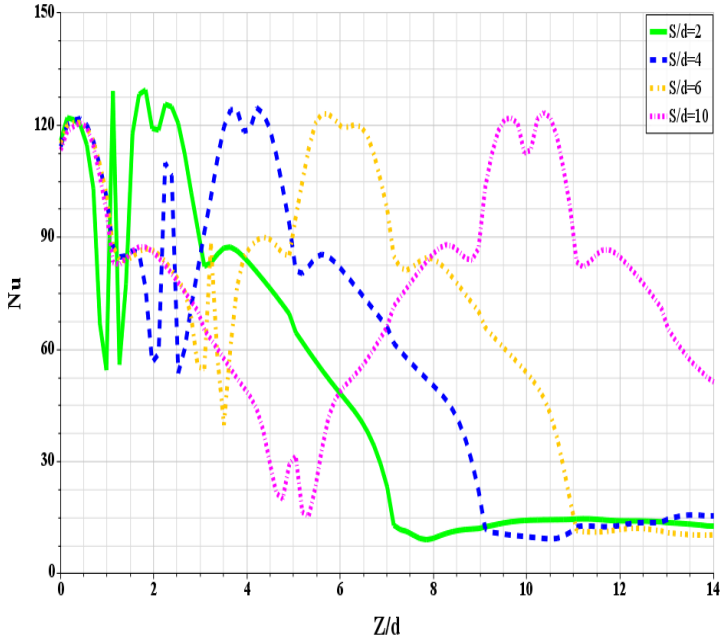

Fig. 14 Effects of the jet to jet spacing on the local Nu along Z-axis (Re=23000, H/d=2, and VR=0.28)

The surface motion has more effect on the heat transfer distribution for a high jet to jet spacing (S/d>2) and it has no significant effect for S/d=2 where the jet impingement flow is very complex due to the strong jet interaction (see Fig.14 and 15).

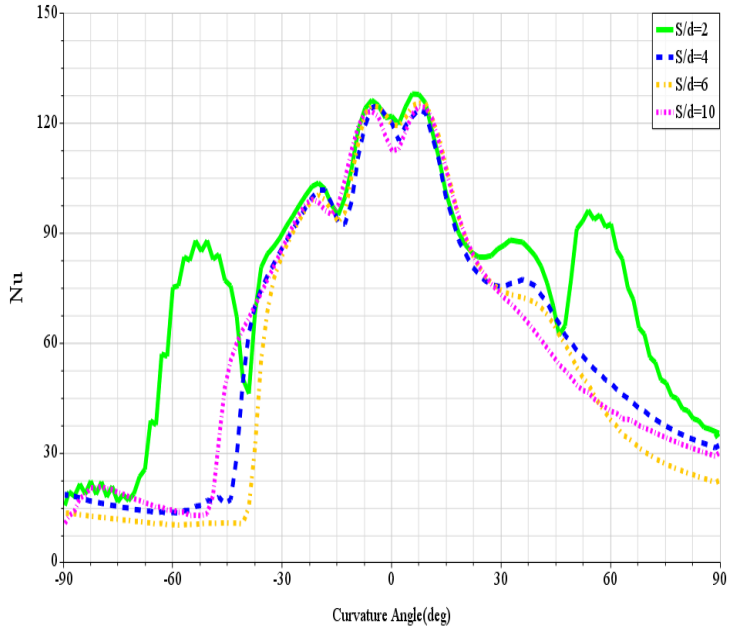

Fig. 15 Effects of the jet to jet spacing on the local Nu along curvilinear axes (Re=23000, H/d=2, VR=0.28)

3.4.2 Effect on Pressure Force

Figure 16 compares the effect of the jet to jet spacing (S/d) on the pressure force coefficient on a moving curved surface. Results indicate that the pressure force coefficients on a moving curved surface are relatively insensitive to the jet to jet spacing within the range examined.

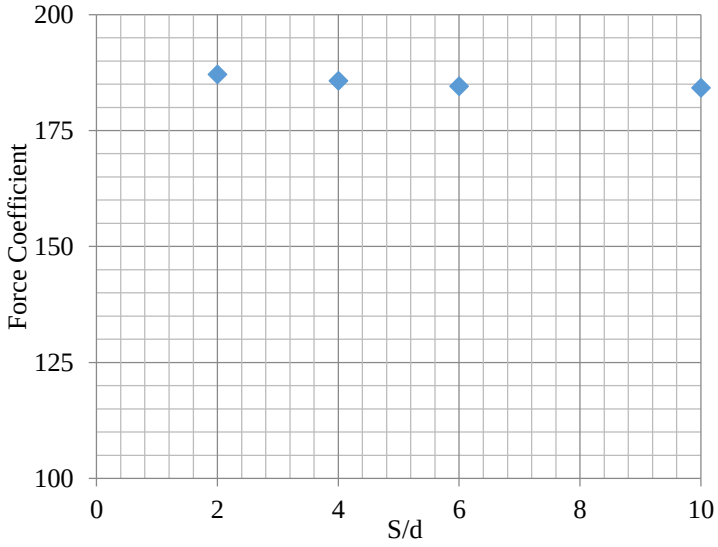

Fig. 16 Effects of the jet to jet spacing on the pressure force coefficient (Re=23000, H/d=2, and VR=0.28)

3.5 Jet Angle

3.5.1 Effect on Heat Transfer

Figure 17 shows the variation of the averaged Nusselt number on a moving curved surface with the jet exit angle (between 45° and 90° as measured with respect to the horizontal axes). Averaged Nusselt number varies quite strongly with jet angle and the averaged value of the Nusselt number sharply increases with an increase in the jet angle. This result is in agreement with the finding of Chitsazan et al. (2020) for jet impingement heat transfer on a flat surface.

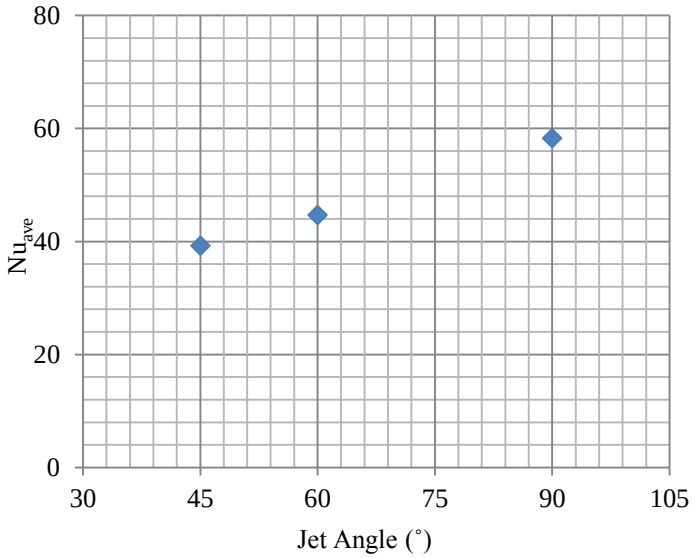

Fig. 17 Effects of jet angle on the average Nu (Re=23000, H/d=1, S/d=4 and VR=0.28)

The heat transfer performance of the jet nozzles is largely improved by the normal impinging jets (θ=90°) compared to the angled jets (see Fig.17) because the local Nu curves for angled jets exhibit a more asymmetrical trend compared to the normal jets (see Fig.18). Hence, the surface motion has a minor effect on the local Nusselt number distribution on a moving curved surface for normal jets compared to the angled jets and the heat transfer is more uniform for angled jets. Thus the importance of surface motion to optimize the heat transfer due to an array of impinging jets is reduced for normal jets.

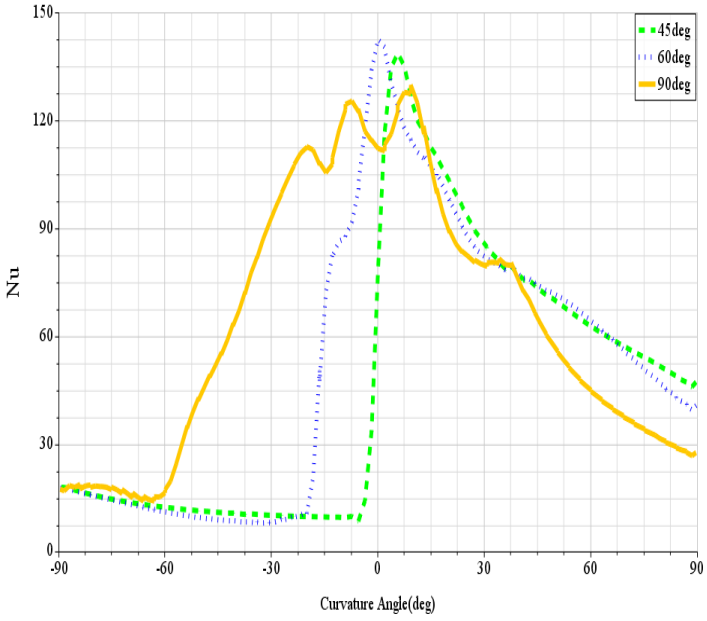

Fig. 18 Effect of jet exit angle on the local Nu along curvilinear axes (Re=23000, H/d=1, S/d=4, and VR=0.28)

3.5.2 Effect on Pressure Force

Figure 19 compares the effect of jet exit angle (ɵ) on the pressure force coefficient on a moving curved surface. The pressure force coefficient is highly dependent on the jet exit angle and increases with increasing the jet exit angle. This result is in agreement with the findings of Chitsazan et al. (2020) for jet impingement force on a flat surface.

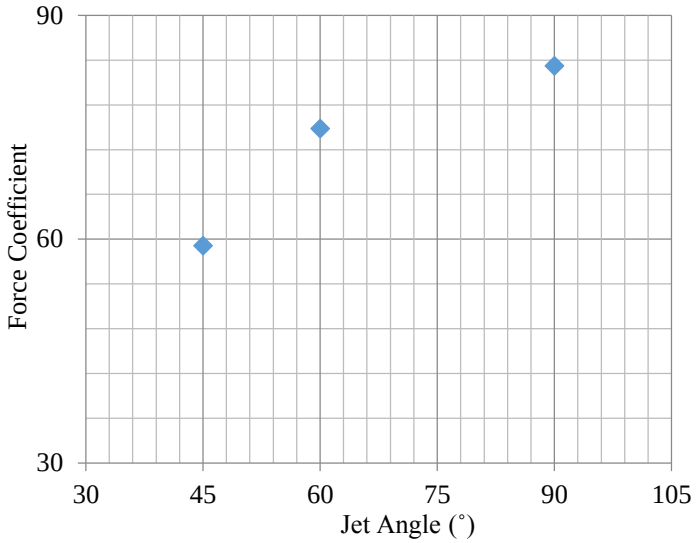

Fig. 19 Effect of jet exit angle on the pressure force coefficient (Re=23000, H/d=1, S/d=4, and VR=0.28)

The pressure force coefficient correlates strongly with the vertical component of the jet flow. With decreasing the jet exit angle, the vertical component decreases, and the parallel component to the wall increases and strengthens the crossflow effect. Hence, when the jet is directed normally to the surface (90°); it can exert the most pressure upon striking the surface (see Fig. 20).

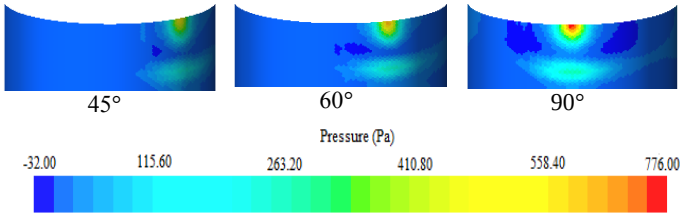

Fig. 20 Pressure distribution from central jet impinging on a moving curved surface for different jet exit angle (Re=23000, H/d=1, S/d=4, and VR=0.28)

3.6 Correlation Equations

Two correlations are developed by a multiple regression fit for the averaged Nu number (Nu_{ave}) and pressure force coefficient (C_f) for the multiple impinging jets on a curved surface:

$$Nu_{ave} = 0.084\,Re^{0.6}(H/d)^{-0.046}(S/d)^{0.194}\theta_{rad}^{0.825}(1+VR)^{-0.0237}(1+Cr)^{-0.461} \quad (10)$$

$$C_f = 0.69\,Re^{0.0152}(133.6H/d^{-0.094} - 2.5H/d - 43.83)(S/d)^{-0.00416}\theta_{rad}^{0.6}(1+2.7VR)^{-0.03}(1+0.7Cr)^{-0.024} \quad (11)$$

The above correlations are proposed in terms of Re, H/d, S/d, θ, VR, and Cr as the independent variables for Re number in the range of 1980 to 66200, H/d from 1 to 20, S/d from 2 to 10, θ from 45 to 90°, VR from 0 to 0.28 and Cr from 0 (flat surface) to 0.8. The observed trends in the numerical simulations are shown by the exponents of the independent parameters in the developed correlations. The agreement between the predicted results by the numerical simulation and correlations is found to

be reasonable and all the data points deviate from the correlation by less than 6% (R^2=0.97) and 5% (R^2=0.98) for the Nu_{ave} and C_f respectively (see Fig. 21 and 22).

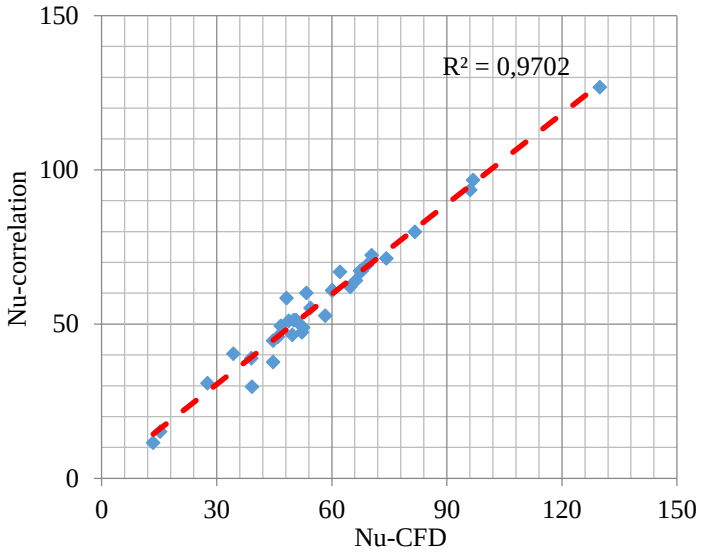

Fig. 21 Parity plot showing a comparison between the average Nu predicted by the CFD and correlation

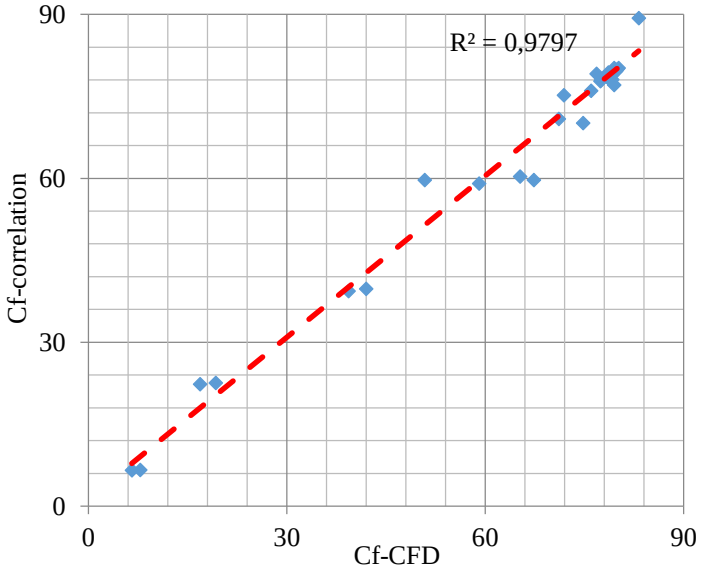

Fig. 22 Parity plot showing a comparison between the force coefficient predicted by the CFD and correlation

4. CONCLUSION

Numerical simulations of multiple circular jets impinging on a fixed curved surface are carried out and validated against the experimental data. The commercial CFD package STAR CCM$^+$ is employed with the SST k-ω turbulence model. This article presents full CFD calculations of the heat transfer between multiple impinging circular jets and a moving curved surface. The effect of jet Reynolds number, jet exit angle, the distance between the jet nozzles to surface, and jet to jet spacing on the heat transfer and pressure force performance have been evaluated. The results are as follows:

The surface motion effects become more pronounced on the Nu number distribution as the Reynolds number decreases and there is more uniform heat transfer for jets at low Reynolds number (e.g. Re=1980 and10000). The results show that the average Nu number on a moving curved surface increases as Re increases.

The surface motion has more effect on the Nu number distribution at the high nozzle to surface distance and there is more uniform heat transfer for jets at the high nozzle to surface distance (H/d=15 and 20). The results show that the average Nu number on a moving curved surface increases as H/d decreases.

The surface motion has more effect on the Nu number distribution on a moving curved surface at the high jet to jet spacing (S/d>2) and the heat transfer is more uniform for jets at high S/d. The average Nu number sharply decreases with a decrease in the jet to jet spacing due to more jet interaction.

The surface motion has a minor effect on the Nu number distribution on a moving curved surface for normal jets compared to the angled jets and the heat transfer is more uniform for angled jets. The average value of the Nu number sharply increases with an increase in the jet exit angle.

The pressure force coefficient on moving curved surfaces is highly dependent on the jet to surface distance (H/d) and jet exit angle (θ) but relatively insensitive to the jet Re number and jet to jet spacing (S/d). Therefore, identification of optimum H/d and θ is very important for the sensitive product to jet force to reduce the force on the surface to zero, thereby providing a very gentle drying or cooling/heating performance for stress-sensitive products.

Two correlations describing the Nu_{ave} and the C_f have been developed as a function of Re, H/d, S/d, θ, VR and Cr. The agreement between the CFD and correlation is found to be reasonable.

NOMENCLATURE

A_f	open area ratio, total jet area to heat transfer area
A	surface area (m^2)
C_f	force coefficient
d	jet diameter (m)
F	force (N)
H	nozzle-to-target spacing (m)
k_t	thermal conductivity (W/m·K)
Nu	Nusselt number
P	pressure (pa)
q	convective heat flux (W/m^2)
R_1	minor curvature radius (m)
R_2	major curvature radius (m)
Re	Reynolds number (Re=Vd/ν)
S	jet pitch (m)
S_x	streamwise jet-to-jet distances (m)
S_y	spanwise jet-to-jet distances (m)
T	temperature (K)
T_t	Reynolds stress tensor
$\overline{U}$	average velocity (m/s)
U_i	instantaneous components of the velocity vector in the direction X_i (m/s)
U_i'	fluctuating components of the velocity vector in the direction Xi (m/s)
X, Y, Z	coordinates
V	magnitude of jet exit velocity (m/s)
y+	dimensionless wall distance

Greek letters

θ	jet exit angle (°)
ν	kinematic viscosity (m^2/s)
ν_t	turbulent viscosity (m^2/s)
ε	dissipation rate (m^2/s^3)
ω	specific dissipation rate (1/s)

ρ	density (kg/m^3)
δ_{ij}	kronecker delta
S_{ij}	mean strain rate tensor (m/s^2)
Θ	general scalar variable
Γ_Θ	diffusivity of Θ (m^2/s)

Subscripts

Ave	average
j	jet
w	wall

Abbreviation

Cr	curvature ratio; the ratio of minor to the major radius
CFD	computational fluid dynamic
GCI	grid convergence index
VR	velocity ratio; surface to jet velocity
SST	shear stress transport

Reference

Ashok Kumar, M., Prasad, B. V. S. S. S., 2009, "Computational investigations of flow and heat transfer on an effused concave surface with a single row of impinging jets for different exit configurations,"*In ASME Turbo Expo 2009: Power for Land, Sea, and Air*, 149-159. https://doi.org/10.1080/19942060.2009.11015289

Bu X., Peng L., Lin G., Bai L., Wen D., 2015, "Experimental study of jet impingement heat transfer on a variable-curvature concave surface in a wing leading edge," *J. Heat and Mass Transfer*, 90, 92-101. https://doi.org/10.1016/j.ijheatmasstransfer.2015.06.028

Chattopadhyay H., 2006, "Effect of surface motion on transport processes due to circular impinging jets – a numerical study," *J. Drying Technology*, 24, 1347-1351. https://doi.org/10.1080/07373930600951117

Chitsazan, A., Glasmacher, B., 2020, "Numerical investigation of heat transfer and pressure force from multiple jets impinging on a moving flat surface," *Int. J. Heat and Technology*, 38, 601-610. https://doi.org/10.18280/ijht.380304

Fenot, M., Dorignac E., Vullierme J.-J., 2008, "An experimental study on hot round jets impinging a concave surface," *J. Heat and Fluid Flow*, 29, 945–956. https://doi.org/10.1016/j.ijheatfluidflow.2008.03.015

Heo, M. W., Lee, K. D., Kim, K. Y., 2012, "Parametric study and optimization of staggered inclined impinging jets on a concave surface for heat transfer augmentation," J. Numerical Heat Transfer, Part A: Applications, 61, 442-462. https://doi.org/10.1080/10407782.2012.654453

Ito, R., Takeishi, K., Oda, Y., Yoshida, N., 2007, "Heat transfer for round air jets flowing along a concave surface," *In ASME/JSME 2007 Thermal Engineering Heat Transfer Summer Conference collocated with the ASME 2007 InterPACK Conference*, 597-605. https://doi.org/10.1115/HT2007-32616

Kadiyala P.K., Chattopadhyay H., 2017, "Numerical simulation of transport phenomena due to array of round jets impinging on hot moving surface," *J. Drying Technology*, 35, 1742-1754. https://doi.org/10.1080/07373937.2016.1275672

Kastner W. and Rippel R., 1988, "Jet impingement forces on structures - experiments and empirical calculation methods," *J. Nuclear Engineering and Design*, 105, 269−284. https://doi.org/10.1016/0029-5493(88)90249-X

Li XC, Corder PP., 2008, "Characteristics of cooling of the leading edge with a row of dual impinging jets," *ASME. Heat Transfer Summer Conference*, 2, 625-633. https://doi.org/10.1115/HT2008-56347

Page, R. H., Hadden, L. L., and Ostowari, C., 1989, "Theory for radial jet reattachment flow," *J. AIAA*, 27, 1500-1505. https://doi.org/10.2514/3.10294

Page, R. H., Carbone, J., and Ostowari, C., 1990, "Radial jet reattachment force," *J. Exp. Fluids*, 8, 13-17. https://doi.org/10.1007/BF00187233

Peper F., Leiner W., Fiebig M., 1997, "Impinging radial and inline jets: A comparison with regard to heat transfer, wall pressure distribution, and pressure loss," *J. Experimental Thermal and Fluid Science*, 14, 194–204. https://doi.org/10.1016/S0894-1777(96)00066-0

Roache P. J., 2003, "Conservatism of the grid convergence index in finite volume computations on steady-state fluid flow and heat transfer," *J. Fluids Engineering*, 125, 731–735. https://doi.org/10.1115/1.1588692

STAR-CCM+ 13.02.013 user guide by CD-Adapco.

Thiele, E. W., Dautel, S. W., Page, R. H., and Seyed-Yagoobi, J., 1993, "A new paper machine drying concept: A multifunctional, radial-jet reattachment nozzle blow box," *TAPPI papermakers conference*, 76, 203-207.

Thiele, E. W., Seyed-Yagoobi, J., Page, R. H., and Castillo-Garcia, H., 1995, "Enhancement of drying rate, moisture profiling and sheet stability on an existing paper machine with RJR blow boxes," *TAPPI papermakers conference, Chicago*, 223-228.

Wang, X. K., Niu, G. P., Yuan, S. Q., Zheng, 2015, J. X., Tan, S. K., 2015, "Experimental investigation on the mean flow field and impact force of a semi-confined round impinging jet,", *J. Fluid Dynamics Research*, 47(2), 025501. https://doi.org/10.1088/0169-5983/47/2/025501